Ductile flow in sub-volcanic carbonate basement as the main control for edifice stability: new experimental insights

Richard R. Bakker[1], Marie E.S. Violay[1,2], Philip M. Benson[1,3] and Sergio C. Vinciguerra[4,5,6]

[1] Geological Institute, ETH Zürich, Swiss Federal Institute of Technology, Zürich, Switzerland

[2] Laboratory of Experimental Rock Mechanics, Station 18, CH-1015 Lausanne, Switzerland

[3] Rock Mechanics Laboratory, School of Earth and Environmental Sciences, University of Portsmouth, United Kingdom.

[4] Department of Geology, University of Leicester, United Kingdom.

[5] British Geological Survey, Keyworth, Nottingham, United Kingdom

[6]Department of Earth Sciences, University of Turin, Italy

Corresponding author: R.R. Bakker, ETH Zürich, NO E 17, Sonneggstrasse 5, Zürich, CH-8092. (richard.bakker@erdw.ethz.ch)

Highlights:

- High P/T triaxial deformation experiments on pure calcite limestone.
- Triaxial experiments in open and closed conditions at 600 and 800 ˚C
- Permeability decreases from ~10^{-17} to ~10^{-19} m^2 between 200 and 600 ˚C
- Decarbonation is strongly limited at high P/T-conditions for pure calcite rocks.

Abstract

Limestone in volcanic basements has been identified as a hazard in terms of edifice stability due to the propensity of calcite to decompose into lime and CO_2 at high temperatures (>600 ˚C), causing a decrease in mechanical strength. To date, such hypotheses have been tested by experiments performed at ambient pressure. The present work determines the mechanical strength of limestone under sub-volcanic conditions of pressure and temperature and evaluates the effect of calcite decomposition. To this end, we use Mt. Etna as a case study, deforming sub-Etnean carbonate samples under tri-axial compression using a Paterson deformation apparatus. We evaluate the effect of thermal decomposition of calcite on sample strength by comparing closed and open systems and measuring the permeability evolution under static conditions. Mechanical and micro-structural observations at a constant strain rate of 10^{-5} s^{-1} and at a confining pressure of 50 MPa indicate that the rocks are brittle up to and including 300 ˚C. At higher temperatures the deformation becomes macroscopically ductile, i.e., deformation is distributed throughout the sample. The brittle to ductile transition is accompanied by an irreversible permeability decrease from ~10^{-17} to ~10^{-19} m^2 between 200 and 600 ˚C. We present new evidence that permanent change in permeability is due to ductile processes closing the initial pore space. Samples deformed at temperatures up to 900 ˚C do not contain any decarbonation products. At these temperatures, permeability is sufficiently low to permit CO_2 pore pressures to increase, thereby increasing local CO_2 fugacity, which in turn strongly limits the decarbonation reaction. We note that, for non-pure calcite rocks, permeability might be sufficient to allow decarbonation reactions to occur. As such, variability in lithologies may slightly influence the efficiency of decarbonation reactions. We conclude that, in a closed system, the instability of Mt. Etna is related to high temperature induced ductile flow of basement limestone rather than chemical / mineralogical changes. This may have important implication for the stability of volcanoes within carbonate-rich

basement, as carbonates become significantly weak at high temperatures, which may increase the risk of sector collapse.

Keywords:

Volcanic Basement, Carbonates, Deformation, Decarbonation, Permeability, HPT Experiments

1. Introduction

Volcanic edifices are the result of accumulation of deposits from effusive and/or explosive eruptions (Odbert et al., 2015). However, their heterogeneity and rapid growth promote instability: in the worst-case scenario this might result in sector collapse (e.g. Mt. St. Helens, Christiansen & Peterson, 1981). Such instabilities are complex and likely result from the interplay between magmatic processes, active tectonics and gravitational collapse. The consequences of sector collapse are often catastrophic and may subsequently trigger new volcanic unrest. This can take the form of rapid influx of magma, as shown for Soufrière Hills Volcano, Monserrat (Cassidy et al., 2015), or increasing the eruptive potential of a magma due to decompression (e.g. Alidibirov and Dingwell, 1996). For this reason, deformation of volcanic edifices and their basements are actively monitored though varied methods such as GPS (Segall and Davis, 1997; Bonacorso et al., 2011), INSAR (e.g. Hooper et al., 2004) and location of local earthquakes (e.g. McNutt, 2005.). These measurements are important in monitoring and forecasting edifice stability and to infer the physical mechanisms taking place in the subsurface.

Previous work has suggested that the overall stability of volcanic edifices is controlled by the properties of their shallow structure along with that of the basement on which they are built (van Wyk de Vries & Borgia, 1996). A thorough understanding of the subsurface geology in terms of its mechanical behavior of the involved lithologies is therefore critical when attempting to link surface deformation to sub-surface processes. Several volcanic edifices, such as El Chichon, Mexico (Duffield et al, 1984), Merapi, Indonesia, (Troll et al., 2012), Vesuvius, Italy (Iacono-Marziano et al., 2009) and Etna, Italy (Mollo et al., 2011; Heap et al., 2013) are built on a carbonate basement. In the case of Mt. Etna, the edifice is made of $<\sim 2$ km thick lavas and pyroclasts unconformably covering a sedimentary basement, which is part of the fold and thrust belt developed at the margin of the Africa promontory during the

Neogene Quaternary Europe-Africa convergence (Wiesmaier et al., 2015). This basement comprises a ca. 2 km thick stack of Miocene thrust sheets of clays, sandstones and carbonates, collectively known as the Apenninic-Maghrebian Chain (AMC) (Branca et al., 2011). These thrust sheets rest on the foreland domain, a thick Mesozoic to Mid-Pleistocene carbonate succession, collectively called the Hyblean Plateau (Catalano et al., 2004).

In general, volcanic basements are subjected to anomalously high geothermal gradients, i.e. a relatively shallow rock mass (~2 km) can be at higher temperatures than normal, ranging between 50-150 ˚C/km as reported for Icelandic geotherms (Flóvenz and Saemundsson, 1993). This is further enhanced by the existence of dykes and sills carrying magma to relatively cool country rocks, especially in areas where layered media exist of differing mechanical properties (e.g. Gudmundsson and Loetveit, 2005). The lithological contrast between volcanic deposits and basement carbonates, along with the large thermal gradients and complex geological structures at depth, generates a complex strength profile.

Mt. Etna possesses an unstable eastern flank, which has been a topic of extensive study (e.g. Apuani et al., 2013). A combination of different monitoring techniques has revealed large-scale deformation at depth (e.g. Lundgren et al., 2004; Neri et al., 2004), supporting the hypothesis that a large detachment exists at depth (4-5 km) within the carbonates (e.g. Acocella and Puglisi, 2013) and more potential detachment surfaces between 1.5 and 3 km depth (e.g. Palano et al., 2008; Nicolosi et al., 2014). To further our understanding of the carbonate basement of Mt. Etna, recent studies have conducted rock deformation experiments (e.g. Mollo et al., 2011; Heap et al., 2013; Wiesmaier et al., 2015). Whilst such data are important to gain first order insights into the mechanical processes of the sedimentary units beneath Mt Etna, the experiments of the aforementioned studies were conducted under

107 uniaxial conditions (i.e. room pressure). To obtain a more complete understanding, such
108 studies need to be extended to higher pressure and temperature conditions. However these are
109 difficult to obtain due to the challenging pressure and temperature conditions that exist in
110 volcanic areas (e.g. Flóvenz, Ó. G., & Saemundsson, K., 1993).
111
112 From a thermo-chemical perspective, carbonate rocks are prone to thermal decomposition by
113 the breakdown of calcite when exposed to temperatures over 600 ˚C (Rodriguez-Navarro et
114 al., 2009); such temperatures are easily reached in volcanic settings. This process is known as
115 decarbonation and implies the decomposition of calcite ($CaCO_3$ into lime (CaO) and carbon
116 dioxide (CO_2) (Mollo et al., 2013 and references therein). The expelled carbon dioxide can
117 potentially enrich nearby magmatic bodies (e.g. Marziano et al., 2007; Chiodini et al. 2011)
118 contributing to the overall CO_2 decarbonation, which is considered a reliable marker of
119 impending eruptions (e.g. Aiuppa et al., 2006). Furthermore, CO_2 can build up directly as
120 local pore pressure, changing the effective confining pressure and subsequently affect the
121 mechanical behavior of the sample. For example, as the brittle ductile transition is pressure
122 dependent, a reduction in effective confining pressure could cause a switch from ductile to
123 the brittle regime. Such mechanisms subsequently change the strength of the volcanic edifice
124 in general. In any case, the key parameter controlling the pore pressure is the permeability,
125 which indirectly determines how easily the gas can escape from the rock. Permeability is
126 notably affected by deformation during which the internal structure of rocks is modified (e.g.
127 Fischer & Paterson, 1992; Zhu and Wong, 1997). Furthermore, deformation is changed by
128 elevated pore pressure as the effective stresses are reduced. Local pore pressures may
129 significantly increase when the permeability is low, especially in the case of isolated pores
130 (e.g. Zhang et al., 1994).
131

Previous studies have investigated the effect of temperature on the strength of carbonate rocks from the basement of Mt. Etna, but they have been limited to unconfined conditions (Mollo et al., 2011; Heap et al., 2013). In Mollo et al. (2011), brittle behavior was seen in all experiments up to 760 ˚C, with a noticeable trend of decreased total strain before failure as temperature increased. Conversely, Heap et al. (2013) reported brittle-ductile transition (BDT) at approximately 550 ˚C. In this work, the BDT is defined as the transition from a loss of strength during strain accumulation to strain accumulation without loss of strength (see Byerlee, (1968) and Rutter, (1986)). Both Mollo et al., (2011) and Heap et al, (2013) indicate thermal decomposition by the presence of the mineral portlandite in post-test sample analysis, which itself formed due to lime reacting with ambient water. To confirm this observation, Mollo et al., (2012) studied thermal decomposition within a closed system (i.e. no free outflow of CO_2) by controlling the carbon-dioxide fugacity during experiments. They found that decarbonation is arrested in a closed system and argued that closed systems might not be realistic due to thermal microcracking, whereby any CO_2 produced would likely escape through the enhanced permeability due to the microcracks. However, these experiments were conducted at ambient pressure (an effective pressure of zero) in the CO_2 fugacity experiments (Mollo et al., 2012). Therefore, these results may not reflect the process at depth where confining pressure, temperature and differential stresses would influence the physio-mechanical behavior of the rock mass.

One of the most extensively studied rocks for which reliable mechanical data exists are carbonates (e.g. Rutter 1995; Renner & Evans, 2002). Many experiments have focused on single crystals or single-phase aggregates of typical minerals such as calcite (e.g. Wang et al., 1996; De Bresser & Spiers, 1997). However deformation of a natural assemblage from a volcanic area have received less attention in literature. The goal of this study is to extend the previous work to high confining pressure and temperatures. Moreover, we aim to better

157 understand how elevated pressure/temperature conditions affect the rheological behavior of
158 carbonates and investigate the thermo-chemical reaction in the carbonates beneath the Etnean
159 volcanic system. The work focuses on a temperature range from 25˚C to 900 ˚C and
160 confining pressures from 50 to 100 MPa (depth equivalent 2-4 km). We additionally assess
161 how high temperatures may modify the permeability of sub-volcanic carbonates.
162
163

2. Material and Methods

2.1 Sampling Material

We used Comiso Limestone (hereafter CL), part of the large succession of thick Mesozoic to Mid-Pleistocene carbonates of the foreland area (Hyblean Plateau, Fig.1). Cross sections suggest that the CL can be found at 4-6 km below Mt. Etna's peak (Branca et al., 2011), although rock types similar to CL may occur at shallower levels whereas large carbonate lenses are also known in the subsurface units (Wiesmaier et al., 2015).

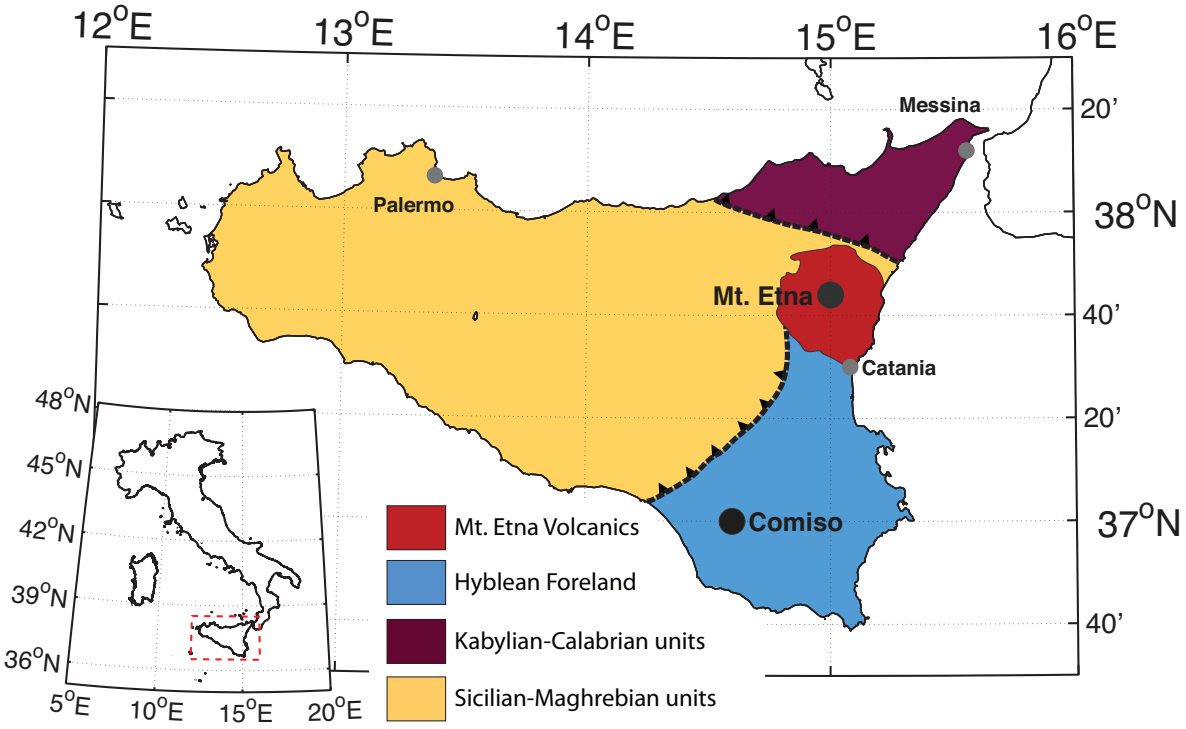

Figure 1: Simplified geological map of Sicily. After Manzi et al., 2011.

The CL formation outcrops 50 km to the south of Mt. Etna and is quarried for building purposes. Sample blocks were obtained from a quarry near the town of Comiso (36˚56'58.3''N, 14˚36'53.6''E; Fig. 1). The formation consists mainly of mud- and wackstones with occasional beds of dolomite and marls. The mineralogical composition has been characterized by XRD (see methods and results). Spectra indicate the samples consist purely of calcite (see figure 5). Pre-test sample characterization using a texture goniometer

180 (Seifert–Scintag XDS2000, installed at ETH Zurich, Geological Institute) established that the
181 samples have an isotropic fabric, and we therefore treat the samples as homogeneous. The
182 initial bulk density of the samples used in this study was 2468 kg/m^{-3} with an initial
183 connected porosity of 8.7%, measured using a helium pycnometer.
184

185 ## 2.2 Methods

186 ### 2.2.1 Sample and assembly preparation

187 Cylindrical samples were drilled using a diamond coring drill of either 12 mm or 15 mm
188 inside diameter and cut to a 2.5 to 1 standard length-to-diameter ratio using a diamond blade
189 saw. All samples used in this study are all drilled from the same block. End faces were
190 ground perpendicular to the coring direction and plane parallel to within 0.01 mm. Samples
191 were stored in a drying oven at 70 ˚C for at least 24 hours to ensure that they were completely
192 dry. Deformation experiments were performed using the "Paterson" type triaxial cell
193 (Paterson, 1990) installed at the Rock Deformation Laboratory at ETH Zürich. Using an
194 internal furnace and Argon as confining medium, the apparatus can reach pressure and
195 temperature (P/T) conditions up to 600 MPa and 1200 °C respectively. Samples are held
196 between alumina and zirconia pistons and the entire assembly jacketed using copper or iron
197 to isolate the sample and pore pressure (if applicable) from the confining medium. To reduce
198 the effect of jacket strength, copper jackets were used at experiments below 700 ˚C and iron
199 jackets at higher temperature, as copper becomes too weak.

200 ### 2.2.2 Triaxial deformation experiments

201 Conditions of interest were chosen as confining pressures at 50 and 100 MPa without
202 imposing pore pressure, and a temperature range of 20-900 °C, spanning the anomalously
203 steep (hot) geotherm found in volcanic areas. The highest temperature of 900 °C would

represent that close to the magmatic plumbing system (although not in direct contact), while 200 – 400 °C would represent more distal parts of the volcanic basement. The depth range investigated here does not strictly represent the depth range where the CL formation occurs underneath Mt. Etna. The Hyblean plateau is inferred to start at a depth of about 4 to 5 km underneath the volcano with an average thickness of about 10 km (e.g. Tibaldi and Groppelli, 2002). This implies our confining pressure corresponds to the shallow parts of CL at depth. However carbonates is ubiquitous within the volcano's sedimentary basement (starting at 1.5 km, (Branca et al., 2011)), thus the confining pressure is of relevance for the upper part of the volcanic edifice.

Triaxial deformation experiments were performed in open (permitting free outgassing to the atmosphere) and closed (sealed environment, constant volume) conditions. In open conditions samples were in contact with the atmosphere on top and bottom faces of the sample, by 2 mm diameter holes. These are present in the middle of the ceramics and assembly used to apply a pore pressure to the sample and place a thermocouple close to the sample. In closed conditions we placed non-porous ceramic spacers on either side of the sample, which are impermeable on experimental timescale. To ensure there were no leaks along the interfaces of the spacers with pistons, we additionally ran tests where a thin copper plate was placed in between, thick enough to seal but not thick enough to influence the mechanical data.

The furnace is pre-calibrated to ensure little to no thermal gradient across the sample length (max 0.2 °C/mm). During all the experiments a constant heating/cooling rate of 15 ˚C/min was used, slow enough to heat up the sample relatively homogeneously, thereby preventing thermal cracking, but still fast enough to reach the experiment conditions quickly. Once the desired P/T conditions were reached and stabilized (~15 minutes), the axial piston was driven to achieve a constant strain rate of 10^{-5} s^{-1}; Force was measured via an internal load cell

measuring differential axial load up to a maximum of 80 kN. This corresponds to a maximum differential stress of roughly 700 MPa across a 12 mm diameter sample (~450 MPa at 15 mm). Piston displacement was measured simultaneously using internal linear variable displacement transducers (LVDTs), in order to calculate sample strain. The total strain of all experiments was kept below ca. 12%, beyond which stress became heterogeneously distributed in the sample due to influence of the upper and lower pistons. Raw data were processed to correct for jacket strength (estimated from Frost and Ashby (1982)), change in sample diameter due to deformation (barreling effect), and distortion due to machine stiffness and deformation in zirconia and alumina pistons.

2.2.3 Permeability tests

The apparatus was equipped with a pore pressure system, comprising of up- and downstream pore-pressure sensors connected to either end of the sample assembly (see also Violay et al., 2015). In the upstream circuit, the system is fitted with a servo-controlled volumometer that may be used in both hydrostatic conditions as well as during deformation tests (i.e. differential stress applied). This system permits pore pressure control and permeability determination via the transient step method (Brace et al., 1968).

Using the method described above, we measured gas permeability at an effective pressure of 50 MPa (a confining pressure of 75 MPa and an equilibrium pore pressure of 25 MPa, assuming a simple effective pressure law). A pore pressure difference of 5 MPa between upstream and downstream reservoirs was applied; the decay of this pressure change with time was fitted with an inverse exponential decay in order to calculate the permeability (Brace et al., 1968). The transient flow depends on the pressure difference and on the volumes of the upstream and downstream reservoirs, which are 8600 and 2260 mm^2, respectively. The small volume changes of the reservoirs, due to pressure changes, have been neglected due to the significant storage capacity and high rigidity of both reservoirs. Pressure changes due

254 temperature variations have also been neglected since the reservoirs are sufficiently far from
255 the “hot zone”, i.e. where the sample sits. We have evaluated the effect of gas slippage
256 (Klinkenberg, 1941), and found that the mean gas pressure was high enough (>3 MPa) to be
257 negligible for permeability determinations (Peach, 1991).
258 In gas permeability measurements, particular care must be taken to seal the surface within the
259 jacket. We decided not to use room temperature as the initial temperature due to the fact that
260 calibration runs with impermeable test samples (metal cylinders) revealed leaks between
261 sample and jacket. It was found that 200 ˚C represented an optimum balance between sealing
262 the jacket via the rheological properties of copper and conditions shallow enough to represent
263 a low end-member for investigation. To mitigate leaks and ensure full saturation of the
264 sample, the sample assembly was held at a confining pressure of 75 MPa and a pore pressure
265 of at least 8 MPa, at room temperature, for at least 12 hours before heating up the assembly
266 and measurements were conducted. We measured the permeability at different stages of a
267 temperature cycle while maintaining a constant effective pressure. Temperature was stepwise
268 increased from 200 to 300, 400, 500 and finally 600 ˚C. If the time to reach equilibrium
269 between reservoirs was sufficiently low (less than 30 minutes), the permeability was
270 measured twice to evaluate data repeatability. The upper temperature limit was imposed due
271 to the use of the copper jacket, chosen for its superior sealing properties between the jacket
272 and the sample and therefore crucial for such low permeability experiments. Finally, to check
273 for hysteresis effects, additional permeability measurements were made during the decreasing
274 temperature cycle at 400 and 200 ˚C. Measurements at temperatures higher than 600 ˚C were
275 conducted using iron jackets, as iron was found to be sealing from 700 ˚C onwards.
276 Given the time-dependent nature of the transient flow method, we only measured
277 permeability under static conditions as sample mechanical relaxation (when in the flow
278 regime, particularly at high temperature) and sample porosity healing impede accurate

279 permeability measurements during deformation. Even in hydrostatic conditions time
280 dependant deformation might occur at high pressure and temperature, however we assume
281 these processes to be much slower than the timescale of our permeability measurement.
282 Indeed following Renner and Evans (2002), under our permeability measurement conditions
283 time dependant mechanisms are activated at 10^{-7} s^{-1}, at which the timescale to reach 1% strain
284 is two orders of magnitude faster than a permeability measurement.

285 **2.2.4 XRD analysis**

286 The starting material as well as tri-axially deformed samples were analyzed using an X-ray
287 diffractometer (Bruker, AXS D8 Advance, equipped with a Lynxeye superspeed detector, as
288 installed at ETH, Institute for Geochemistry and Petrology). For post-test samples the XRD
289 spectra were obtained within hours of running the test, such to avoid recrystallization and / or
290 alteration by exposure to ambient water (lime to portlandite). Post-test samples were dry-cut
291 to the dimensions acceptable for XRD analysis.
292 We compared samples held at confinement at different temperatures with two samples held at
293 800 ˚C in an oven at ambient pressure for a similar amount of time, using a similar heating
294 and cooling regime as the samples held confined, to confirm that decarbonation reactions do
295 occur when there is no confining pressure.
296 Obtained XRD spectra were compared with crystal structure data derived from the American
297 Mineralogist Crystal Structure Database (see Downs and Hall-Wallace 2003).
298

3 Results

3.1 Mechanical data

In all experiments, the apparatus and the sample initially deformed elastically (i.e. stress increased linearly with strain) until the yield strength was overcome and permanent deformation of the sample initiated. Static Young's modulus was determined by fitting a 1st order polynomial to the stress-strain curve between 0.2 and 0.6-0.8 % strain. The lower limit was imposed to reduce non-linear behavior resulting from closure of any residual space between piston and sample, as well as the crack closure threshold, the upper limit by the yield point (i.e. strain at which yielding occurred) (Brace, 1966).

For the room temperature (20 ˚C) experiment, Young's modulus was approximately 34 (+/- 2) GPa, decreasing to 16 (+/- 2) GPa as temperature is increased to 600 ˚C. We found that the Young's modulus is independent of the confining pressure (supplementary material, item 3). At a confining pressure of 50 MPa and temperatures between 20 and 300 °C, samples yield around 300 MPa and 1% strain. Peak stress was at 375, 390 and 430 MPa, and at 1.6, 2.5 and 7.0% strain, for the 20, 200 and 300 °C experiments, respectively. Strain weakening occurred after peak stress until the samples eventually formed a shear-fracture. In all these experiments, a common feature is the increase in the total strain before failure as temperature increases, as evidenced by the strain at which a sudden stress drop occurred (2.5, 4.5 and 8% for experiments at 20, 200 and 300 ˚C). After failure, continuous deformation was recorded with a differential stress of 250 to 280 MPa. In the case of the experiment conducted at 200 ˚C, a clear stick-slip frictional behavior was observed.

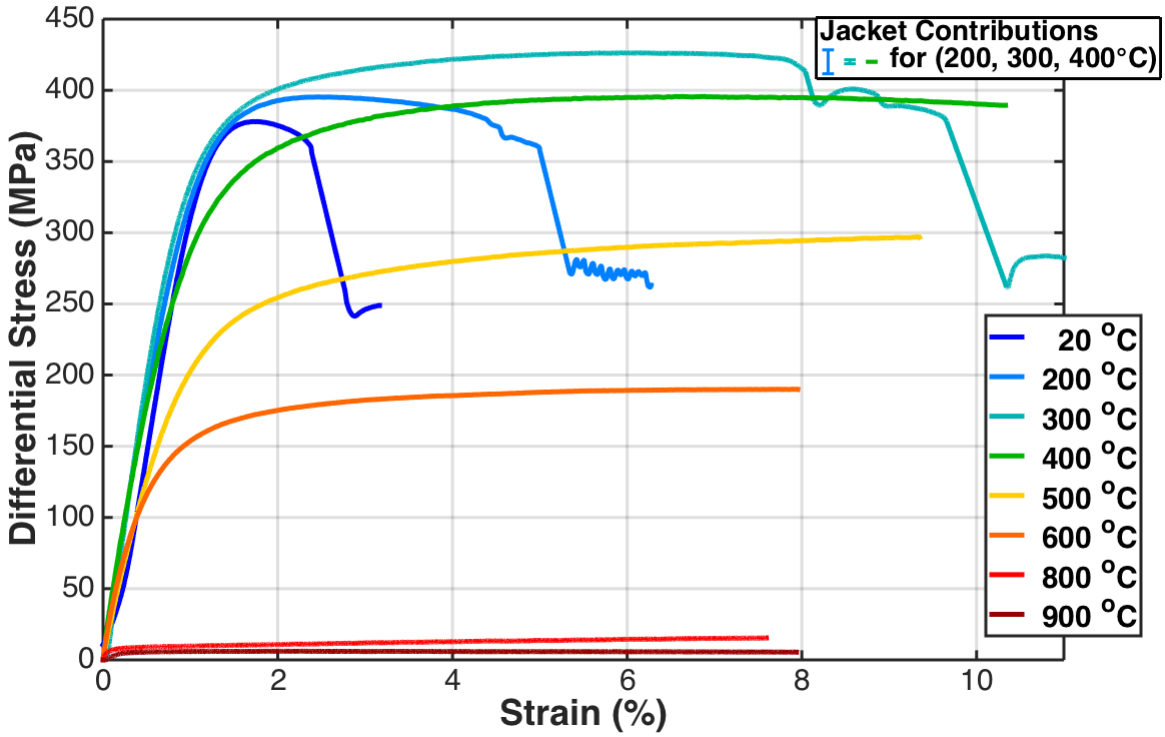

Figure 2: Differential stress (MPa) versus Strain (%) curves for Comiso Limestone for different temperatures (indicated by line style and color), all experiments at a P_c = 50 MPa and strain rate = 10^{-5} s^{-1}. Jacket contribution is plotted for experiments at 200, 300 and 400 ˚C, at higher temperatures the contribution is negligible as well as at room temperature where a polymer (heat shrink tube) was used.

Where brittle fracturing occurred up to 300 ˚C, experiments conducted at temperatures in excess of 300 ˚C samples showed macroscopically ductile behavior. The yield point is primarily dependent on temperature, however a secondary dependency (monotonic hardening between 5 to 10 MPa per % strain) has also been measured. The flow stress (measured at 5% strain and at a strain rate of 10^{-5} s^{-1}) decreases from 310, 250, 180 to 10 MPa at temperatures of 400, 500, 600 to 800 ˚C, respectively. A similar behavior was found at 100 MPa confining pressure: increasing temperatures lead to a switch from brittle to ductile behavior (suppl. material). In detail, when comparing two experiments performed at different confining pressures and low temperature (20, 200 ˚C), the yield strength and peak strength both increase with increasing confinement pressure. At 400 and 600 ˚C, we observed macroscopically ductile behavior, with a higher hardening rate at higher confining pressure.

Comparing open and closed conditions (all at 50 MPa of confining pressure): the yield stress and sample strength, as measured at 600 and 800 ˚C, is not influenced by the ability of pore pressures to escape or build up. A very minor change in post peak mechanical behavior was observed (figure 3). For closed systems at 600 ˚C, the stress slowly reaches a maximum of ca. 200 MPa at a finite strain of 8%, compared to a stress of ca. 220 MPa for open system at 600 ˚C. At 800 ˚C we don't observe significant changes, which could be due to the very low sample strength.

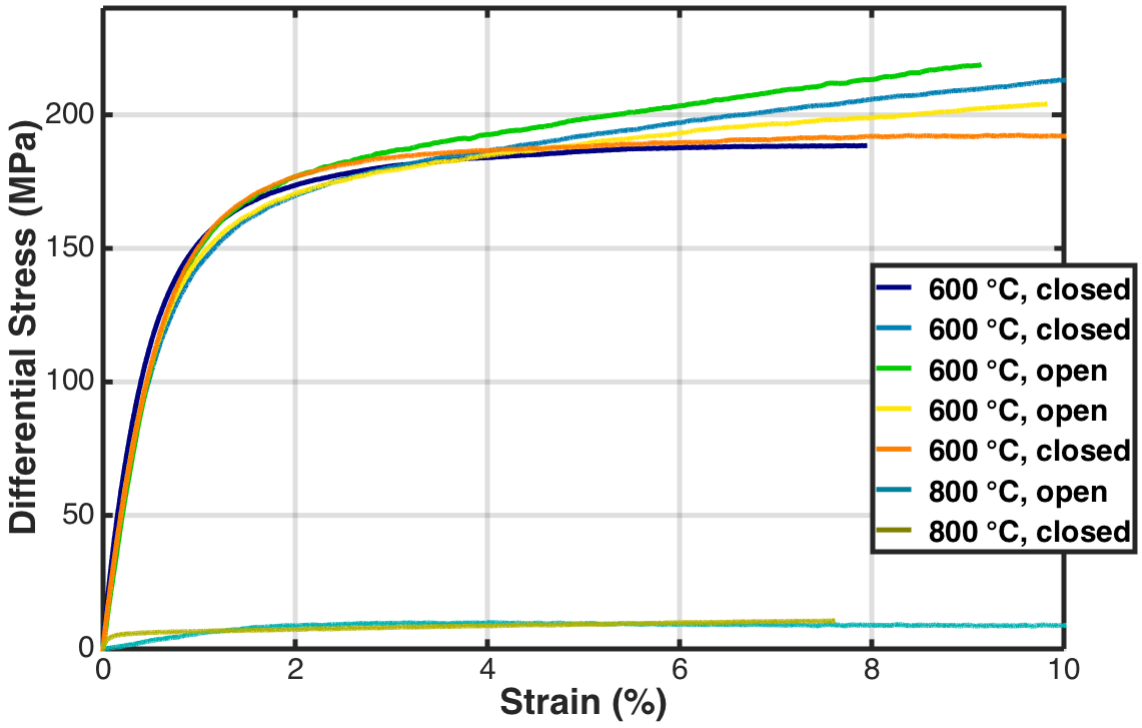

Figure 3: Differential stress (MPa) versus Strain (%) curves for Comiso limestone, all experiments at T = 600 and 800 ˚C and a confining pressure of σ_3 = 50 MPa and a constant strain rate of 10^{-5} s^{-1}. Open refers to drained experiments (free outgassing allowed) and closed to confined (constant volume).

3.2 Deformation textures and microstructures

Post-deformation thin sections were investigated under a Scanning Electron Microscope (SEM, type JEOL-JSM 6300F, installed at ETH Zurich Institute of Geochemistry and Petrology) (Figure. 4). At 25 ˚C strain was localized, generally along a main fault associated with smaller subparallel or intersecting cracks and faults. Most of the cracks were inclined

354 30° to the compression direction. Between 200 ˚C and 300 ˚C about 100 to 500 μm thick
355 anastomosing shear bands developed, most of them at 30 - 40º to the compression direction,
356 the angle increasing with increased temperature. Grain-size reduction, micro-cracking, and
357 rigid-rotation and frictional sliding of fragments can be observed within shear bands.
358 Samples deformed at 400 °C and higher (up to 900 ˚C) are characterized by the absence of
359 strain localization.

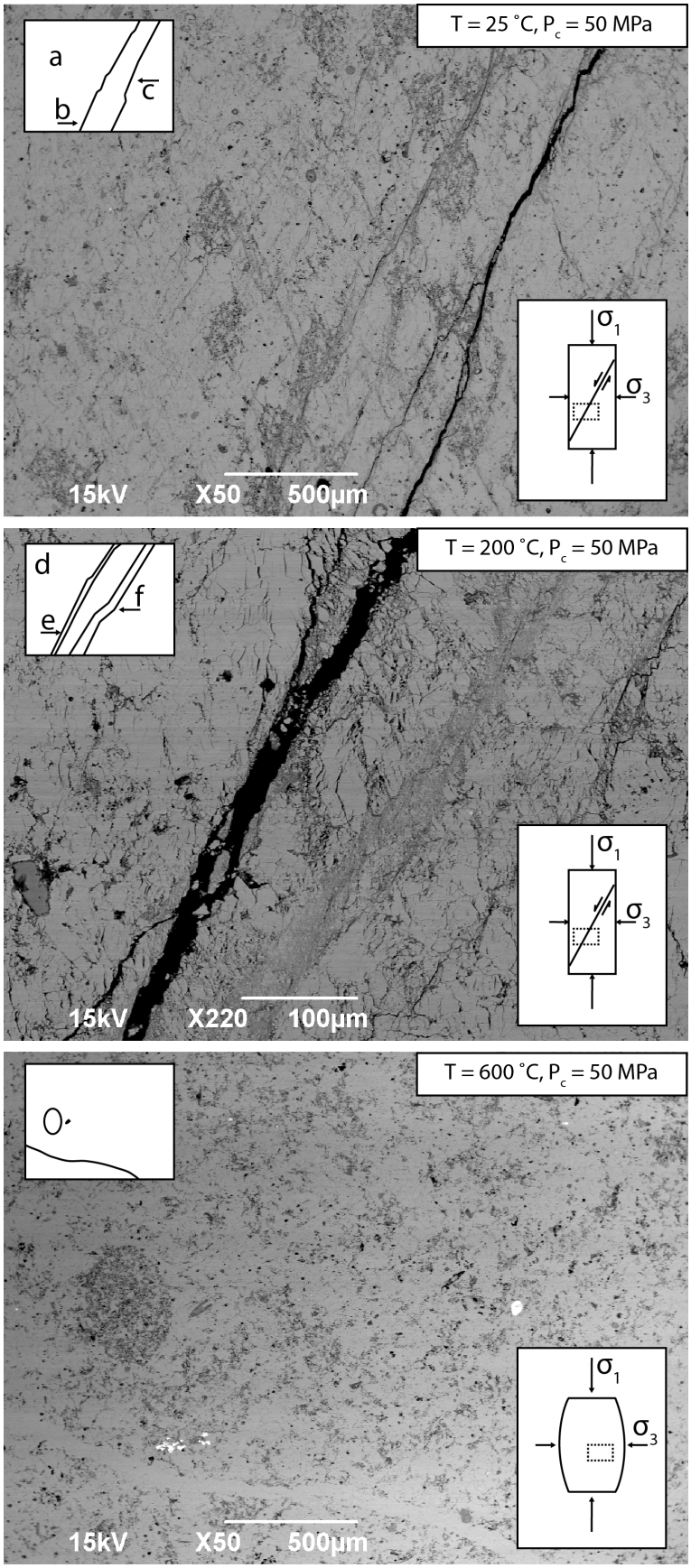

Figure 4: SEM images of post-experiment samples, all deformed at P_c = 50 MPa. Upper panel: sample deformed at room temperature, a) conjugate sets of microcracks, b and c) localization features with c) as main shear fracture.

Middle panel: sample deformed at T = 200 ˚C, similar to top panel, d) microcracks, e) and f) main localization features. Lower panel: sample deformed at 600 ˚C, no significant microcracks or localization features.

3.3 XRD results

Two samples heated up to 800°C in an oven at ambient pressure, show distinctive peaks at two-theta angles associated with lime. In one case some residual calcite could be detected. In contrast, for samples held under a confining pressure at 50 MPa and at temperatures ranging from 500-900 ˚C, XRD data show only the presence of calcite. Peaks for portlandite and lime have not been identified out of the background noise. For the experiments performed at 800 and 900 ˚C, we chose to orient the XRD sample such that end-face of the sample was measured. At this face the sample was connected with the atmosphere by the 2 mm thermocouple feedthrough, however no decarbonation products were detected.

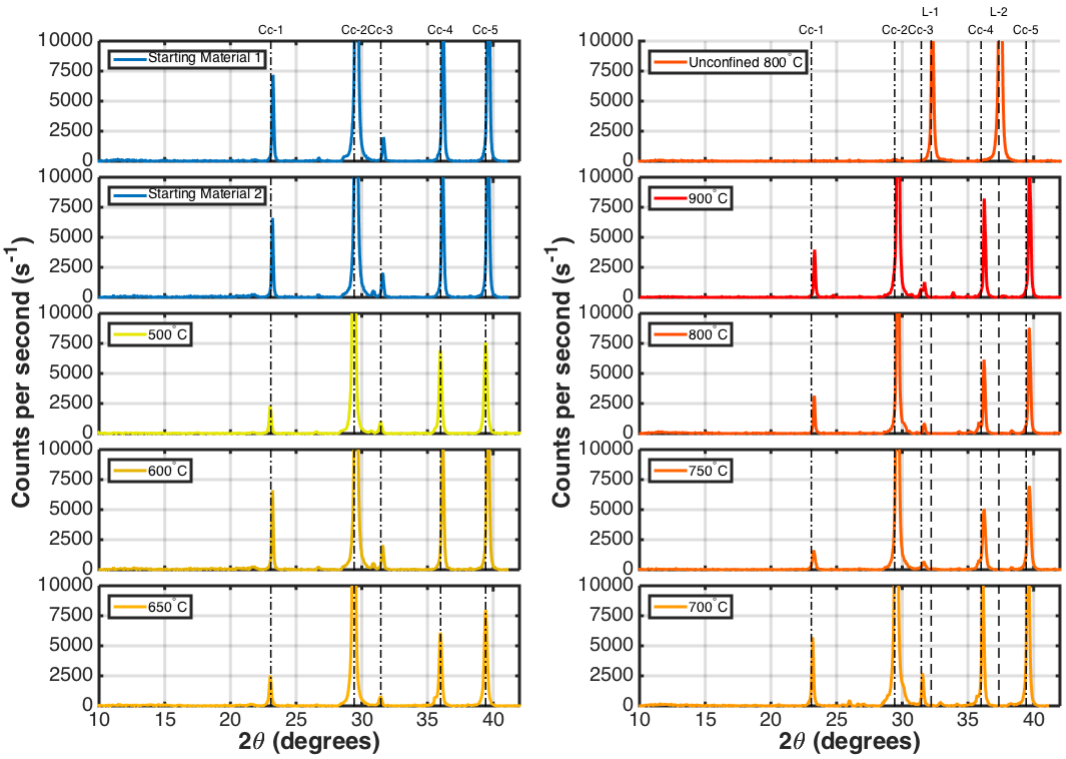

Figure 5: 2-theta spectra derived from XRD measurements of pre- and post-test samples. Peaks are correlated with calcite and lime lattice planes, (respectively CC-# and L-#, data derived from mindat.org), Y-axis (counts per second) is kept constant and relatively low such that minor peaks may be identified, while major peaks plot outside of the

range. Portlandite peaks are to be expected around 2-theta angles of 18° and 35° (Heap et al, 2013). The panel labeled "Unconfined 800 °C" refers to a sample kept in an open system, at 800 °C without effective confinement.

3.4 Permeability

Permeability was measured prior to sample deformation, under hydrostatic stress conditions (P_{eff} = 50 MPa). Permeability decreased with temperature from 1.5 x 10^{-17} m^2 at 200 °C to 3.5 x 10^{-19} m^2 at 600 °C (Fig. 7). The decrease can be described by best-log-linear fit of the form k = 10^(aT+b) with a = -4.5126 x 10^{-3}, b = 15.8829, permeability (k) in m^2 and temperature (T) in °C.

Permeability essentially remains unchanged, at approximately 2 x 10^{-19} m^2, during stepwise sample cooling, implying it is not recoverable. We preformed a second permeability test using an iron jacket, suitable for higher temperature measurements (T>600 °C). This test showed the permeability was too low to be measured by the transient step method, indicating the permeability is probably below 10^{-20} m^2. Post-test porosity measurements of that sample, with helium pycnometer, showed that porosity had decreased to less than 2%.

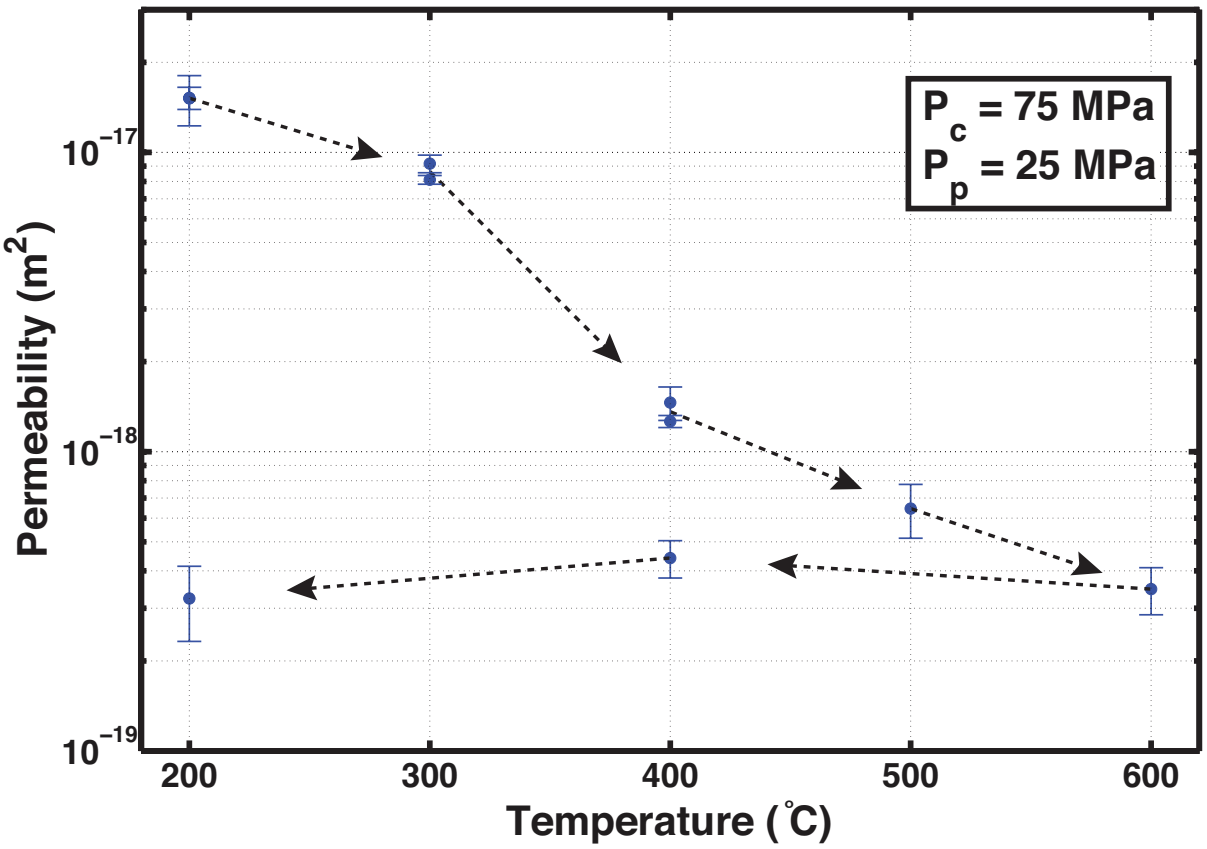

396

397 **Figure 6: Permeability evolution with increasing and subsequently decreasing temperatures as indicated with the**
398 **arrows.**

399

4. Discussion

Decarbonation has been identified as a cause for strength reduction in carbonates exposed to high temperatures (Mollo et al., 2011; Heap et al., 2013), as well as a cause of non-magmatic CO_2–source in magmatic systems (Chiodini et al. 2011). However, decarbonation reactions relevant to volcanic basements in terms of temperature and pressure, have not been evidenced so far. Here, we have assessed the deformation properties of low porosity carbonate rocks at elevated temperatures and pressures, in the context of the volcanic system of Mt. Etna, with special interest on the effect of decarbonation on mechanical strength.

4.1 Comparison with uniaxial experiments

Experiments at confining pressure of 50 MPa documented a distinct change in the nature of faulting with increasing temperature. Changes in the deformation mode correlate with the stress-strain behaviour in both suites of samples: localization corresponds to strain weakening with increasing deformation, whereas distributed deformation corresponds to strain hardening. The degree of localization and grain comminution decreased with temperature. The failure mode changed from wedge splitting (up to 200 ˚C) to shear rupture (up to 300 ˚C, following the classification of Evans and Kohlstedt, 1999) to homogeneous flow (from >300 to 900 ˚C). As different mechanisms of deformation may occur simultaneously, it is difficult to identify their relative roles. However, in our experiments (i.e. 50 MPa of confining pressure and a strain rate of 10^{-5} s^{-1}), the BDT can be placed around 350 +/- 50 ˚C, whereby the BDT is defined as the switch of the material's capacity to deform to a substantial strain without stress drop (Rutter, 1986; Heap et al., 2013). This definition does not imply any particular deformation mechanism. Instead, the definition is a macroscopic characterization of the sample deformation. Previous studies on carbonate bearing rocks predict that distributed deformation at high temperature and confining pressure is mainly accommodated

424 by intracrystalline plasticity and diffusion mechanisms (Rutter 1995; Renner and Evans,
425 2002; Kushnir et al. 2015).
426 Previous work has been conducted on sub-Etnean limestone in uniaxial compressive (UC)
427 experiments (Mollo et al., 2011; Heap et al., 2013). The measured strength (UCS) was lower
428 by a factor of 2 than the strength measured under tri-axial conditions (TCS) (present study).
429 Moreover, for the same laboratory strain rate (10^{-5} s^{-1}), the BDT occurred at approximately
430 150 ˚C lower temperature than under uniaxial compression (500 +/- 50 ˚C; Heap et al., 2013).
431 A likely hypothesis for the lower BDT temperature is a decreased propensity for
432 microcracking, as cracks are harder to open and / or propagate under confining pressure.
433 Moreover plastic deformation mechanisms are more prevalent at higher pressure (Violay et
434 al., 2012).
435 Further differences between the UC and TC are revealed through changes in chemistry of the
436 post-test materials. In UC tests, decarbonation products (lime and/or portlandite) were found
437 in samples exposed to temperatures more than 650 ºC. Decarbonation products were not
438 found in TC tests (open), at comparable temperatures, nor at higher temperatures (up to 900
439 ˚C). More evidence of inhibition of decarbonation reactions arises by the similarity between
440 the open and closed experiments, suggesting that either decarbonation does not significantly
441 influence the sample strength, or it did not occur sufficiently on the timescale of our
442 experiment (several hours). We ascribe the differences in decarbonation between UC tests
443 and TC tests to permeability reduction due to ductile flow of the sample under confining
444 pressure. Ductile deformation leads to the closure of pore connectivity, thereby trapping CO_2
445 in the pores, thus sufficiently increasing local CO_2 fugacity to limit decarbonation reactions
446 (see Mollo et al., 2012). However, in natural cases, if deformation is accompanied by dilation
447 (e.g. dyking events), this might provide sufficient pathways for CO_2 to escape at least
448 transiently, and thereby the decarbonation reaction can occur locally. Note that the

449 sedimentary basement of Mt. Etna also consists of quartzarenites (Wiesmaier et al., 2015).
450 The quartz-components could provide a framework, resisting compaction and thereby
451 allowing a sufficient permeability at PT conditions for decarbonation reactions to occur.
452 Moreover, our tests were conducted on a timescale of several hours. On a geological time
453 scale CO_2 would be able to diffuse out of the sample, even if the permeability is considerably
454 reduced. In such a case it is likely that the local pore pressure and CO_2 fugacity will remain
455 high enough to limit decarbonation reactions, but not to exclude them entirely. To quantify
456 such effects on long timescales is beyond the limitations of our experiment, and would
457 require a setup able to hold samples at stable PT conditions for weeks, months or even years.
458 It should be noted that permeability experiments were only run under static conditions as no
459 reliable results may be obtained with the current setup whilst samples are being deformed.
460 The transient permeability method is time-dependent, which poses a problem in the ductile
461 field where viscous relaxation occurs during the equilibration of the two reservoirs and stress-
462 strain conditions cannot be kept constant. However, axial deformation can potentially change
463 the permeability and subsequently the rate at which CO_2 is liberated. For low porosity rocks,
464 existing laboratory measurements indicate that both dilatancy (porosity increasing with
465 strain) and permeability increases for during brittle failure and subsequent cataclastic flow on
466 the fracture plane (Zoback and Byerlee, 1975; Zhu and Wong, 1997; De Paola et al., 2009).
467 Conversely, for high porosity rocks shear failure may be accompanied by a permeability
468 decrease (e.g. David et al., 1994). In the ductile domain, high porosity rocks can form
469 compaction bands, thereby decreasing the permeability (e.g. Baud et al., 2012), whereas low
470 porosity rocks can be associated with either minor dilatancy or compaction, depending of the
471 deformation mechanism (Violay et al., 2015). Permeability experiments run with a harmonic
472 method (rather than transient flow method) during deformation are desirable to investigate
473 the modifications of pore space induced by deformation.

4.2 Implications for Mt. Etna

Decarbonation in carbonate basement of Mt. Etna has been invoked as a key factor influencing edifice stability (Heap et al., 2013). Our new experimental results suggest that confining pressure, combined with high temperatures representative of volcanic systems, does not significantly alter the mineral composition of carbonates (i.e. no presence of lime instead of calcite) on a laboratory time scale. This is due to a sufficiently lowered permeability. Based on this observation, and considering that ductile deformation is dominant at volcanic temperatures and high confining pressures, we propose that the edifice collapse can be due to ductile flow of limestone at depth. In contrast, the lowered rock strength due to decarbonation reactions suggested by Heap et al. (2013) can only be effective in an open system at shallow levels such that CO_2 is able to diffuse slowly over geological timescales. In deeper parts of the system, the permeability of pure calcite limestone will have significantly decreased such that decarbonation reactions are considerably limited. This in turn causes the rate of strength changes due to decarbonation reactions to decrease. Therefore strength changes at high confinement due to decarbonation reactions (> 600 ˚C) are insignificant compared to the effect of temperature.

Our new results suggest that ductile deformation is likely to be pervasive and widely distributed within Mt. Etna's sedimentary basement at depths of 4-5 km. The conceptual model of Tibaldi and Gropelli (2002) invokes two slip surfaces allow movement of Etna's eastern flank. The shallower of the two is placed within the sub-Etnean clay horizons (e.g. Nicolosi et al., 2014). The deeper surface of the two would be where magma intrusion-induced slip is thought to occur. In this model, most of the deformation is accommodated by these two slip surfaces. Our study suggests that the deformation may be also partially

accommodated by ductile flow of the carbonate unit. This statement fits numerical modeling (Apuani et al. 2013), where a diffuse deformation zone is suggested. However, it should be noted that the presented experiments were done at a limited set of PT conditions, and for a single strain rate. Because the rocks are deforming by both cataclastic and plastic processes, the exact scaling of strength with effective lithostatic pressure, pore-fluid pressure, and deformation rate needs further clarification, which will be treated in a subsequent manuscript. Finally, we have shown that limestone can deform in a ductile manner, involving very low strength, when exposed to high temperatures and high confining pressure. We have also demonstrated that decarbonation reaction are inhibited or at least strongly limited under confining pressure representative of volcanic system. Weaknesses in the volcanic basement can cause sector collapse (van Wyk de Vries & Borgia, 1996). Mechanisms such as involved in Mt. Etna's eastern flank, are likely to occur in other volcanic edifices with carbonate rich basements as well. Indeed, volcanoes with carbonate rich basements often show geomorphological evidence of sector collapse (e.g. El Chichon, Mexico (Duffield et al, 1984), Merapi, Indonesia, (Troll et al., 2012), Vesuvius, Italy (Iacono-Marziano et al., 2009)). However, it should be noted that sector collapse cannot be exclusively explained by ductile flow within the basement, other mechanisms such as fracturing and faulting should be considered (e.g. van Wyk de Vries & Borgia, 1996). Such effects can be quantified by field investigations and numerical modelling.

5. Conclusions

The deep structure of volcanoes control the risk of edifice collapse. Limestone in volcanic basements has been identified as a hazard due to the propensity of calcite to decompose into lime and CO_2 at high temperatures (>600 ˚C), causing a decrease in mechanical strength. In this study, we have performed experiments at pressures and temperature conditions representative of volcano-tectonic settings (i.e. 2-4 km depth and a high temperature range) on pure calcite limestone: Comiso Limestone. Our results show that Comiso Limestone experiences a brittle to ductile transition at 350 +/- 50 ˚C at laboratory strain rates (10^{-5} s^{-1}). New measurements conducted on Comiso Limestone, at temperatures up to and including 900 ˚C while at 50 MPa confining pressure show that, contrary to previous arguments, decarbonation reactions do not occur to a measurable extent under confining pressure on the timescale (hours) of our experiments. There are uncertainties when scaling up to geological timescales, but our results suggest that decarbonation reactions are significantly limited. Decarbonation reactions are limited for the following reasons: 1) high temperatures cause a reduction in rock strength, favoring compaction. 2) compaction leads to the closure of pore network. 3) local pore CO_2–fugacity is able to build up, limiting the decarbonation reaction. We note that our results are also applicable to limestone with a higher initial porosity. However if other carbonate rocks (e.g. with siliciclastic components) sustain a lesser degree of compaction, then the permeability might be sufficient to allow decarbonation reactions. This has important implications in the interpretation of the deformation of Mt. Etna's eastern flank. We propose that deformation is pervasive and mainly accommodated by ductile flow of carbonate basement units.

These new results may have important implication for other volcanoes with carbonate rich basements, where ductile flow at depth may cause a significant increase in the risk of sector collapse.

6. Acknowledgements:

This work is funded by the Swiss National Science Foundation (Project #200021-137867). The authors would like to thank Robert Hofmann for technical support, and members of ETH Zurich's Rock Deformation Laboratory and Alissa Zuijdgeest for insightful discussions. The manuscript has greatly benefited from comments by Jean-Pierre Burg, and much appreciated constructive reviews by Silvio Mollo and Mike Heap.

7. References:

Acocella, V., & Puglisi, G., 2013. How to cope with volcano flank dynamics? A conceptual model behind possible scenarios for Mt. Etna. Journal of Volcanology and Geothermal Research, 251, 137-148.

Aiuppa, A., Federico, C., Giudice, G., Gurrieri, S., Liuzzo, M., Shinohara, H., ... & Valenza, M., 2006. Rates of carbon dioxide plume degassing from Mount Etna volcano. Journal of Geophysical Research: Solid Earth (1978–2012), 111(B9).

Alidibirov, M., & Dingwell, D. B. (1996). Magma fragmentation by rapid decompression. Nature, 380(6570), 146-148.

Apuani, T., Corazzato, C., Merri, A.& Tibaldi A., 2013. Understanding Etna flank instability through numerical models. J. Volc. Geotherm. Res, 251, 112–126.

Bonaccorso, A., Bonforte, A., Calvari, S., Del Negro, C., Di Grazia, G., Ganci, G., ... & Boschi, E., 2011. The initial phases of the 2008–2009 Mount Etna eruption: A multidisciplinary approach for hazard assessment. Journal of Geophysical Research: Solid Earth (1978–2012), 116(B3).

Baud, P., Meredith, P., & Townend, E., 2012. Permeability evolution during triaxial compaction of an anisotropic porous sandstone. Journal of Geophysical Research: Solid Earth (1978–2012), 117(B5).

Brace, W. F., Paulding, B. W., & Scholz, C. H., 1966. Dilatancy in the fracture of crystalline rocks. Journal of Geophysical Research, 71(16), 3939-3953.

Brace, W.F., Walsh, J.B., and Frangos, W.T-., 1968. Permeability of granite under high pressure. Journal of Geophysical research, 73(6), 2225-2236.

Branca, S., Coltelli, M., Groppelli, G., and Lentini, F., 2011. Geological map of Etna Volcano 1:50000 scale, Italian Journal of Geosciences, 130(3), 265-291.

576 Byerlee, J.D., 1968. The brittle-ductile transition in rocks. Journal of Geophysical research,
577 73, 4741–4750
578 Cassidy, M., Watt, S. F. L., Talling, P. J., Palmer, M. R., Edmonds, M., Jutzeler, M., ... &
579 Wang, F., 2015. Rapid onset of mafic magmatism facilitated by volcanic edifice collapse.
580 Geophysical Research Letters.,42 ,4778-4785, doi:10.1002/2015GL064519
581 Catalano, S., Torrisi, S., and Ferlito, C., 2004. The relationship between Late Quaternary
582 deformation and volcanism of Mt. Etna (eastern Sicily): new evidence from the
583 sedimentary substratum in the Catania region. Journal of Volcanology and Geothermal
584 Research, 132(4), 311-334.
585 Chiodini, G., Caliro, S., Aiuppa, A., Avino, R., Granieri, D., Moretti, R., & Parello, F., 2011.
586 First 13C/12C isotopic characterisation of volcanic plume CO2. Bulletin of volcanology,
587 73(5), 531-542.
588 Christiansen, R.L. and Peterson, D.W., 1981. Chronology of the 1980 eruptive activity U.S.
589 Geological Survey Special Paper, 1250 pp. 17–30.
590 David, C., Wong, T. F., Zhu, W., & Zhang, J., 1994. Laboratory measurement of
591 compaction-induced permeability change in porous rocks: Implications for the generation
592 and maintenance of pore pressure excess in the crust. Pure and Applied Geophysics,
593 143(1), 425-456.
594 De Bresser, J. H. P., & Spiers, C. J., 1997. Strength characteristics of the r, f, and c slip
595 systems in calcite. Tectonophysics, 272(1), 1-23.
596 De Paola, N., D. R. Faulkner, Collettini C., 2009. Brittle versus ductile deformation as the
597 main control properties of low-porosity anhydrite rocks, J. Geophys. Res., 114, B06211,
598 doi:10.1029/2008JB005967.
599 Downs, R. T., & Hall-Wallace, M., 2003. The American Mineralogist crystal structure
600 database. American Mineralogist, 88(1), 247-250.

601 Duffield, W. A., Tilling, R. I., & Canul, R., 1984. Geology of El Chichón Volcano, Chiapas,
602 Mexico. Journal of Volcanology and Geothermal Research, 20(1), 117-132.
603 Evans, B., & Kohlstedt, D. L., 1995. Rheology of rocks. Rock Physics & Phase Relations: A
604 Handbook of Physical Constants, 148-165.
605 Fischer, G. J., & Paterson, M. S., 1992. Measurement of permeability and storage capacity in
606 rocks during deformation at high temperature and pressure. International Geophysics, 51,
607 213-252.
608 Flóvenz, Ó. G., & Saemundsson, K., 1993. Heat flow and geothermal processes in Iceland.
609 Tectonophysics, 225(1), 123-138.
610 Frost, H. J., & Ashby, M. F., 1982. Deformation mechanism maps: the plasticity and creep of
611 metals and ceramics.
612 Gudmundsson, A., & Loetveit, I. F., 2005. Dyke emplacement in a layered and faulted rift
613 zone. Journal of Volcanology and Geothermal Research, 144(1), 311-327.
614 Heap, M.J., Mollo, S., Vinciguerra, S.C., Lavallée, Y., Hess, K.-U., Dingwell, D.B., Baud, P.,
615 and Iezzi, G., 2013. Thermal weakening of the carbonate basement under Mt. Etna
616 volcano (Italy): Implications for volcano instability, J. Volc. Geotherm. Res., 250, 42-60,
617 doi: 10.1016/j.volcgeores.2012.10.004
618 Hooper, A., Zebker, H., Segall, P., & Kampes, B., 2004. A new method for measuring
619 deformation on volcanoes and other natural terrains using InSAR persistent scatterers.
620 Geophysical research letters, 31(23).
621 Iacono-Marziano, G., Gaillard, F., Scaillet, B., Pichavant, M., & Chiodini, G., 2009. Role of
622 non-mantle CO2 in the dynamics of volcano degassing: The Mount Vesuvius example.
623 Geology, 37(4), 319-322.
624 Klinkenberg, L. J., 1941. The permeability of porous media to liquids and gases. In *Drilling*
625 *and production practice*. American Petroleum Institute.

626 Kushnir, A. R., Kennedy, L. A., Misra, S., Benson, P., & White, J. C., 2015. The mechanical
627 and microstructural behaviour of calcite-dolomite composites: An experimental
628 investigation. Journal of Structural Geology, 70, 200-216.
629 Lundgren, P., Casu, F., Manzo, M., Pepe, A., Berardino, P., Sansosti, E., & Lanari, R., 2004.
630 Gravity and magma induced spreading of Mount Etna volcano revealed by satellite radar
631 interferometry. Geophysical Research Letters, 31(4).
632 Marziano, G. I., Gaillard, F., & Pichavant, M., 2007. Limestone assimilation and the origin of
633 CO 2 emissions at the Alban Hills (Central Italy): constraints from experimental
634 petrology. Journal of Volcanology and Geothermal Research, 166(2), 91-105.
635 Manzi, V., Lugli, S., Roveri, M., Schreiber, B. C., & Gennari, R. 2011. The Messinian
636 "Calcare di Base" (Sicily, Italy) revisited. Geological Society of America Bulletin, 123(1-
637 2), 347-370.
638 McNutt, S.R., 2005. Volcanic seismology. Annu. Rev. Earth planet. Sci., 32, 461-491.
639 Mollo, S., Vinciguerra, S.C., Iezzi, G., Iarocci, A., Scarlato, P., Heap, M.J., and Dingwell,
640 D.B., 2011. Volcanic edifice weakening via devolatilization reactions, Geophys. J. Int.,
641 186, 1073–1077, doi:10.1111/j.1365-246X.2011.05097.x.
642 Mollo, S., Heap, M. J., Iezzi, G., Hess, K.-U., Scarlato, P. and Dingwell, D. B., 2012.
643 Volcanic edifice weakening via decarbonation: a self-limiting process? Geophysical
644 Research Letters, 36, L15307, doi: 10.1029/2012GL052613.
645 Mollo, S., Heap, M. J., Dingwell, D. B., Hess, K. U., Iezzi, G., Masotta, M., Scarlato, P. and
646 Vinciguerra, S., 2013. Decarbonation and thermal microcracking under magmatic PTf
647 CO2 conditions: the role of skarn substrata in promoting volcanic instability. Geophysical
648 Journal International, ggt265.

649 Neri, M., Acocella, V., Behncke, B., 2004. The role of the Pernicana Fault System in the
650 spreading of Mount Etna (Italy) during the 2002–2003 eruption. Bull. Volcanol. 66(5),
651 417–430, DOI: 10.1007/s00445–003–0322.
652 Nicolosi, I., D'Ajello Caracciolo, F., Branca, S., Ventura, G. and Chiappini, M., 2014.
653 Volcanic conduit migration over a basement landslide at Mount Etna (Italy). Sci. Rep. 4,
654 5293; DOI:10.1038/srep05293.
655 Odbert, H., Taisne, B., & Gottsmann, J., 2015. Deposit loading and its effect on co-eruptive
656 volcano deformation. Earth and Planetary Science Letters, 413, 186-196.
657 Palano, M., Puglisi, G., & Gresta, S., 2008. Ground deformation patterns at Mt. Etna from
658 1993 to 2000 from joint use of InSAR and GPS techniques. Journal of Volcanology and
659 Geothermal Research, 169(3), 99-120.
660 Paterson, M.S., 1990. Rock deformation experimentation. In: Duba, A.G., Durham, W.B.,
661 Handin, J.W., Wang, H.F. (Eds.), The Brittle-Ductile Transition in Rocks. The Heard
662 Volume, American Geophysical Union Geophysical Monograph, 56. AGU, Washington,
663 DC, pp. 187-194.
664 Peach, C.J., 1991. Influence of deformation on the fluid transport properties of salt rocks.
665 Geologica ultraiectina, 77, 1-238.
666 Renner, J., & Evans, B., 2002. Do calcite rocks obey the power-law creep equation?.
667 Geological Society, London, Special Publications, 200(1), 293-307.
668 Rodriguez-Navarro, C., Ruiz-Agudo, E., Luque, A. Rodriguez-Navarro, A. B., Ortega-
669 Huertas, M., 2009. Thermal decomposition of calcite: Mechanisms of formation and
670 textural evolution of CaO nanocrystals. American Mineralogist 94, 578-584
671 Rutter, E., 1986. On the nomenclature of mode of failure transitions in rocks,
672 Tectonophysics, 122, 381- 387.

673 Rutter, E. H., 1995. Experimental study of the influence of stress, temperature, and strain on
674 the dynamic recrystallization of Carrara marble. Journal of Geophysical Research: Solid
675 Earth (1978–2012), 100(B12), 24651-24663.
676 Segall, P., & Davis, J. L., 1997. GPS applications for geodynamics and earthquake studies.
677 Annual Review of Earth and Planetary Sciences, 25(1), 301-336.
678 Tibaldi, A., and Groppelli, G., 2002. Volcano-tectonic activity along structures of the
679 unstable NE flank of Mt. Etna (Italy) and their possible origin, J. Volcanol. Geotherm.
680 Res., 115, 277–302, doi:10.1016/S0377-0273(01)00305-5.
681 Troll, V. R., Hilton, D. R., Jolis, E. M., Chadwick, J. P., Blythe, L. S., Deegan, F. M.,
682 Schwarzkopf, L.M., and Zimmer, M., 2012. Crustal CO2 liberation during the 2006
683 eruption and earthquake events at Merapi volcano, Indonesia. Geophysical Research
684 Letters, 39(11).
685 Van Wyk de Vries, B., & Borgia, A., 1996. The role of basement in volcano deformation.
686 Geological Society, London, Special Publications, 110(1), 95-110.
687 Violay, M., Gibert, B., Mainprice, D., Evans, B., Dautria, J. M., Azais, P., & Pezard, P.,
688 2012. An experimental study of the brittle‐ductile transition of basalt at oceanic crust
689 pressure and temperature conditions. Journal of Geophysical Research: Solid Earth (1978‐
690 2012), 117(B3).
691 Violay, M., Gibert, B., Mainprice, D., & Burg, J. P., 2015. Brittle versus ductile deformation
692 as the main control of the deep fluid circulation in oceanic crust. Geophysical Research
693 Letters, 42(8), 2767-2773.
694 Wang, Z. C., Bai, Q., Dresen, G., Wirth, R., & Evans, B., 1996. High-temperature
695 deformation of calcite single crystals. Journal of Geophysical Research: Solid Earth
696 (1978–2012), 101(B9), 20377-20390.

Wiesmaier, S., Heap, M. J., Branca, S., Gilg, H. A., Kueppers, U., Hess, K. U., ... & Dingwell, D. B., 2015. Variability in composition and physical properties of the sedimentary basement of Mt Etna, Italy. Journal of Volcanology and Geothermal Research, 302, 102-116.

Zhang, S., Cox, S.F., Paterson, M.S., 1994. The influence of room temperature deformation on porosity and permeability in calcite aggregates, J. Geophys. Res., 99, 15761–15775.

Zhu, W., & Wong, T. F., 1997. The transition from brittle faulting to cataclastic flow: Permeability evolution. *Journal of Geophysical Research: Solid Earth (1978–2012)*, *102*(B2), 3027-3041.

Zoback, M. D., & Byerlee, J. D., 1975. The effect of microcrack dilatancy on the permeability of Westerly granite. Journal of Geophysical Research, 80(5), 752-755.

709 Figure Captions:

710 **Figure 1 (width: one column):**

711 Simplified Geological Map of Sicily. After Manzi et al., 2011.

712

713 **Figure 2 (width: one column):**

714 Differential stress (MPa) versus Strain (%) curves for Comiso Limestone for different
715 temperatures (indicated by line style and color), all experiments at a Pc = 50 MPa and strain
716 rate = 10^{-5} s^{-1}. Jacket contribution is plotted for experiments at 200, 300 and 400 ˚C, at higher
717 temperatures the contribution is negligible as well as at room temperature where a polymer
718 (heat shrink tube) was used.

719

720 Figure 3 (width: one column):

721 Differential stress (MPa) versus Strain (%) curves for Comiso limestone, all experiments at T
722 = 600 and 800 ˚C and a confining pressure of σ_3 = 50 MPa and a constant strain rate of 10^{-5} s^{-1}.
723 Open refers to drained experiments (free outgassing allowed) and closed to confined
724 (constant volume).

725

726 Figure 4 (width: one column):

727 SEM images of post-experiment samples, all deformed at Pc = 50 MPa. Upper panel: sample
728 deformed at room temperature, a) conjugate sets of microcracks, b and c) localization
729 features with c) as main shear fracture. Middle panel: sample deformed at T = 200 ˚C, similar
730 to top panel, d) microcracks, e) and f) main localization features. Lower panel: sample
731 deformed at 600 ˚C, no significant microcracks or localization features.

732

733 Figure 5 (width: two columns):

2-theta spectra derived from XRD measurements of pre- and post-test samples. Peaks are correlated with Calcite and lime lattice planes, (respectively CC-# and L-#, data derived from mindat.org), Y-axis (counts per second) is kept constant and relatively low such that minor peaks may be identified, while major peaks plot outside of the range. Portlandite peaks are to be expected around 2-theta angles of 18˚ and 35˚ (Heap et al, 2013). The panel labeled "Unconfined 800 ˚C" refers to a sample kept in an open system, at 800 ˚C without effective confinement.

Figure 6 (width: one column):
Permeability evolution with increasing and subsequently decreasing temperatures as indicated with the arrows.

FIGURES

Figure 1 (color version, web usage)

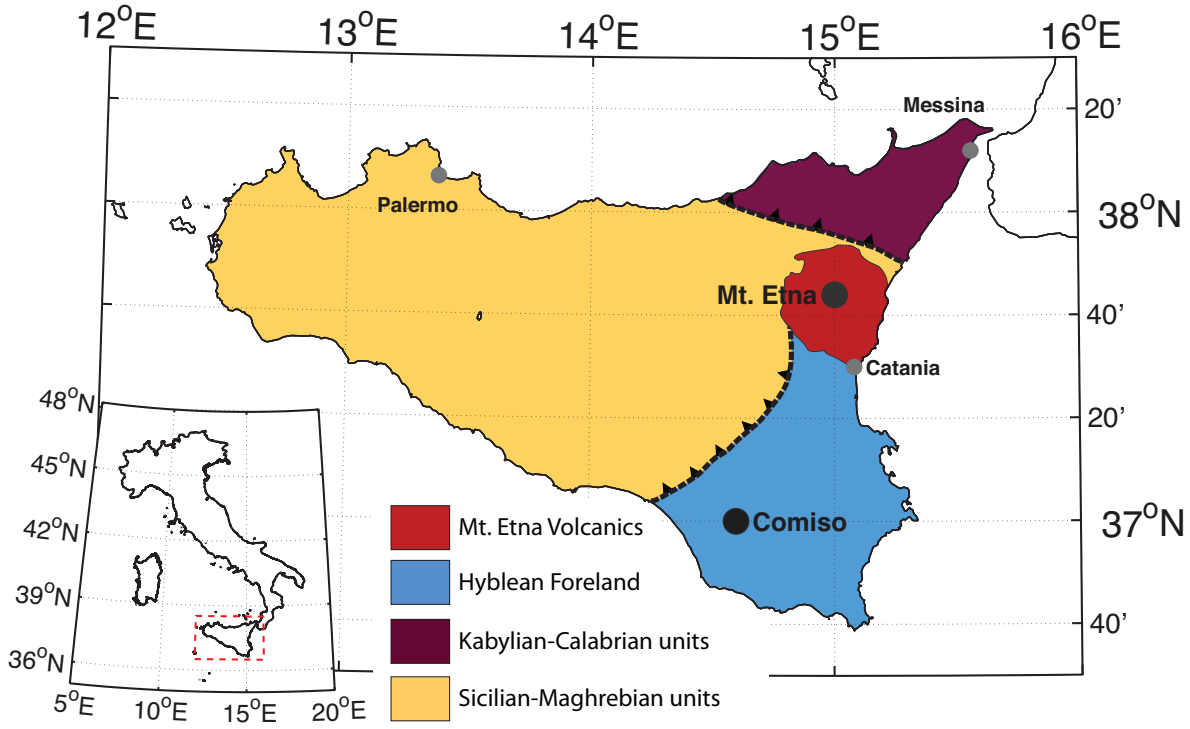

Figure 1 (grayscale, printed version)

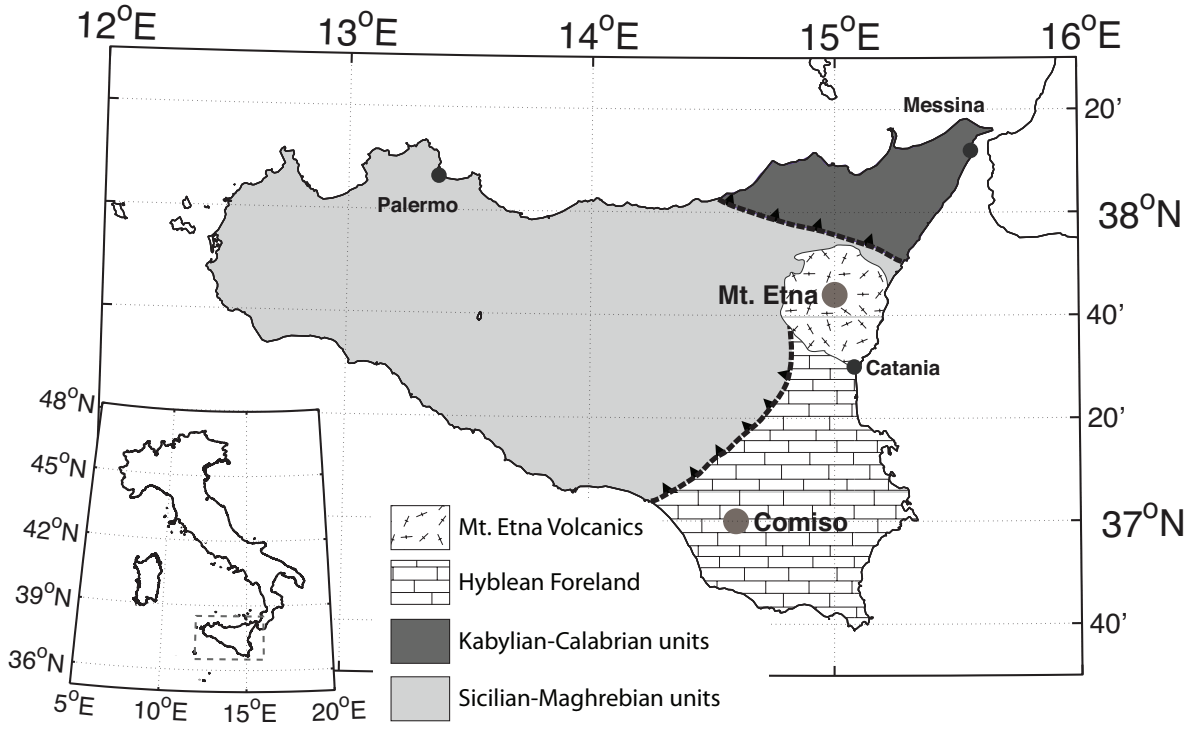

752

753 Figure 2 (color version, web usage)

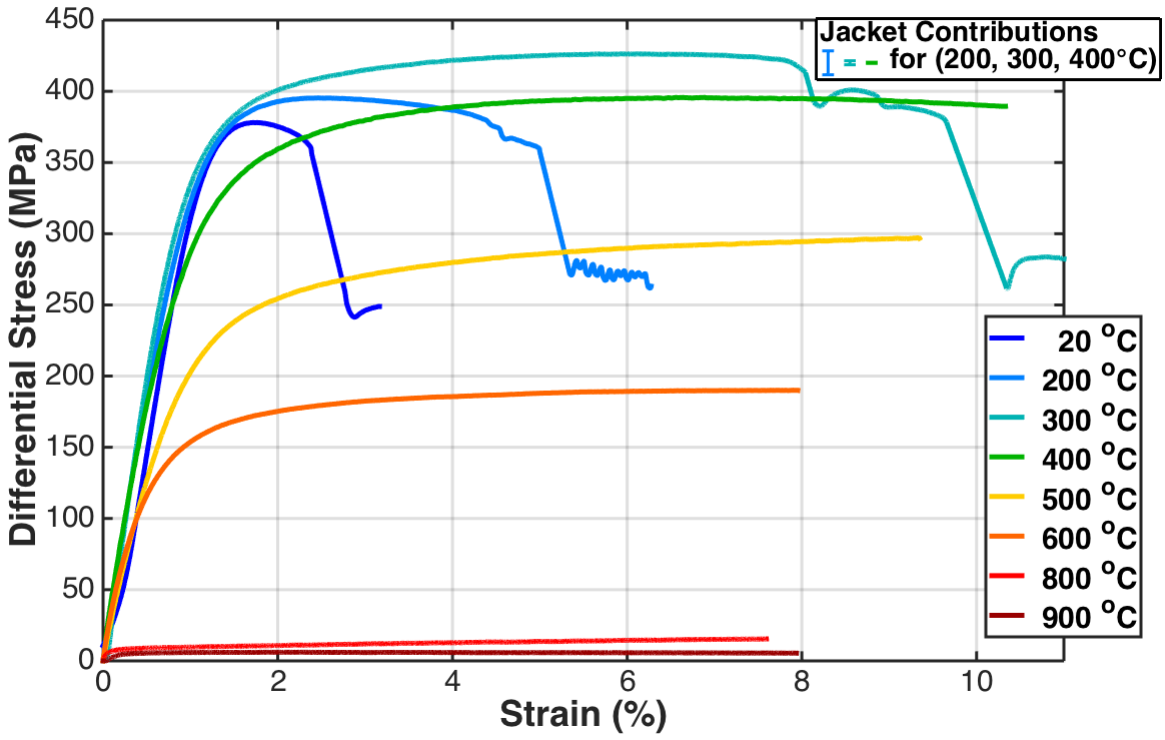

754

755 Figure 2 (grayscale, printed version)

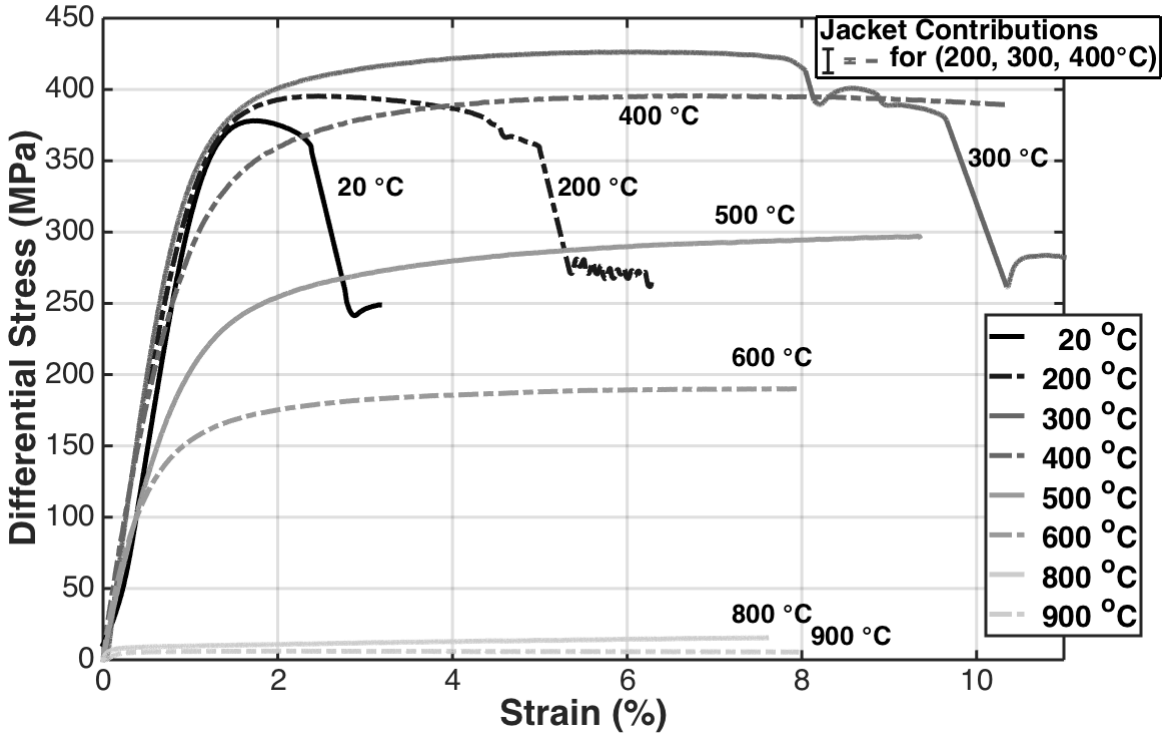

756

757 Figure 3 (color version, web usage)

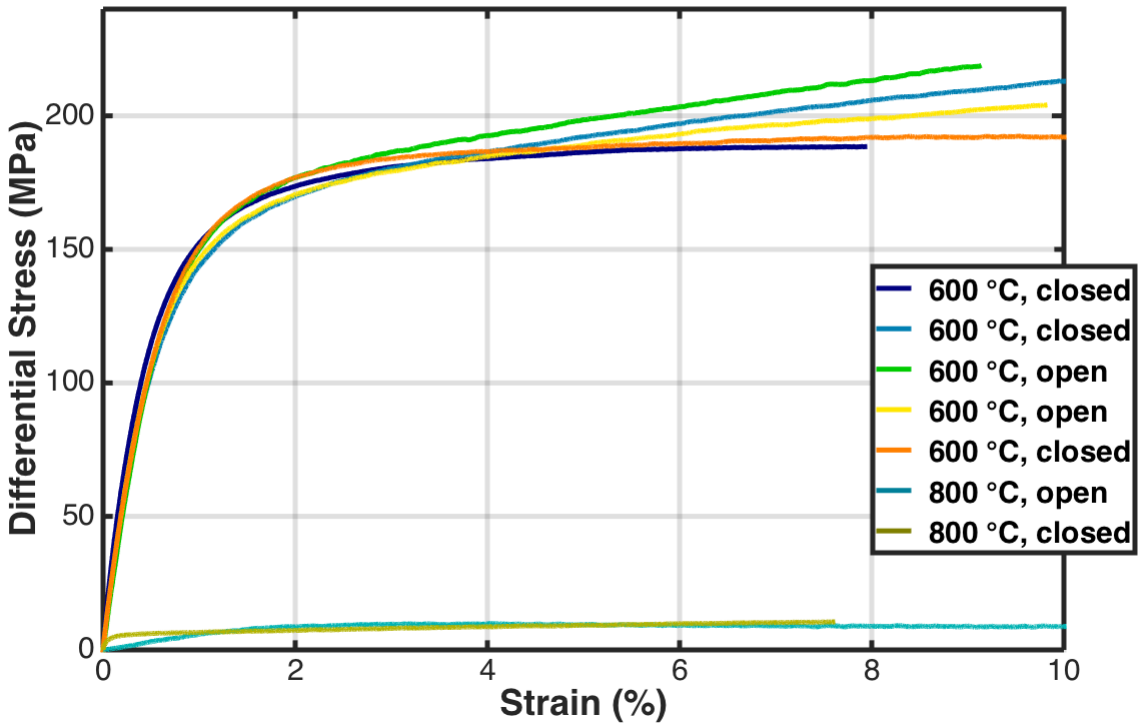

758

759 Figure 3 (grayscale, printed version)

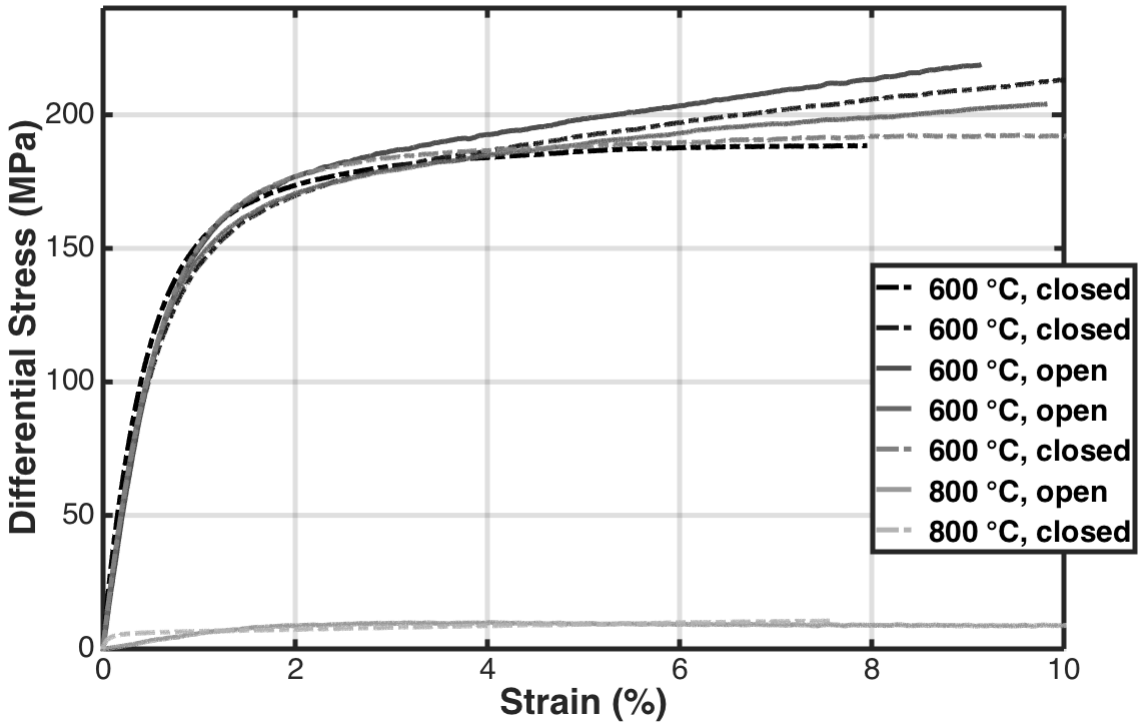

760

761 Figure 4

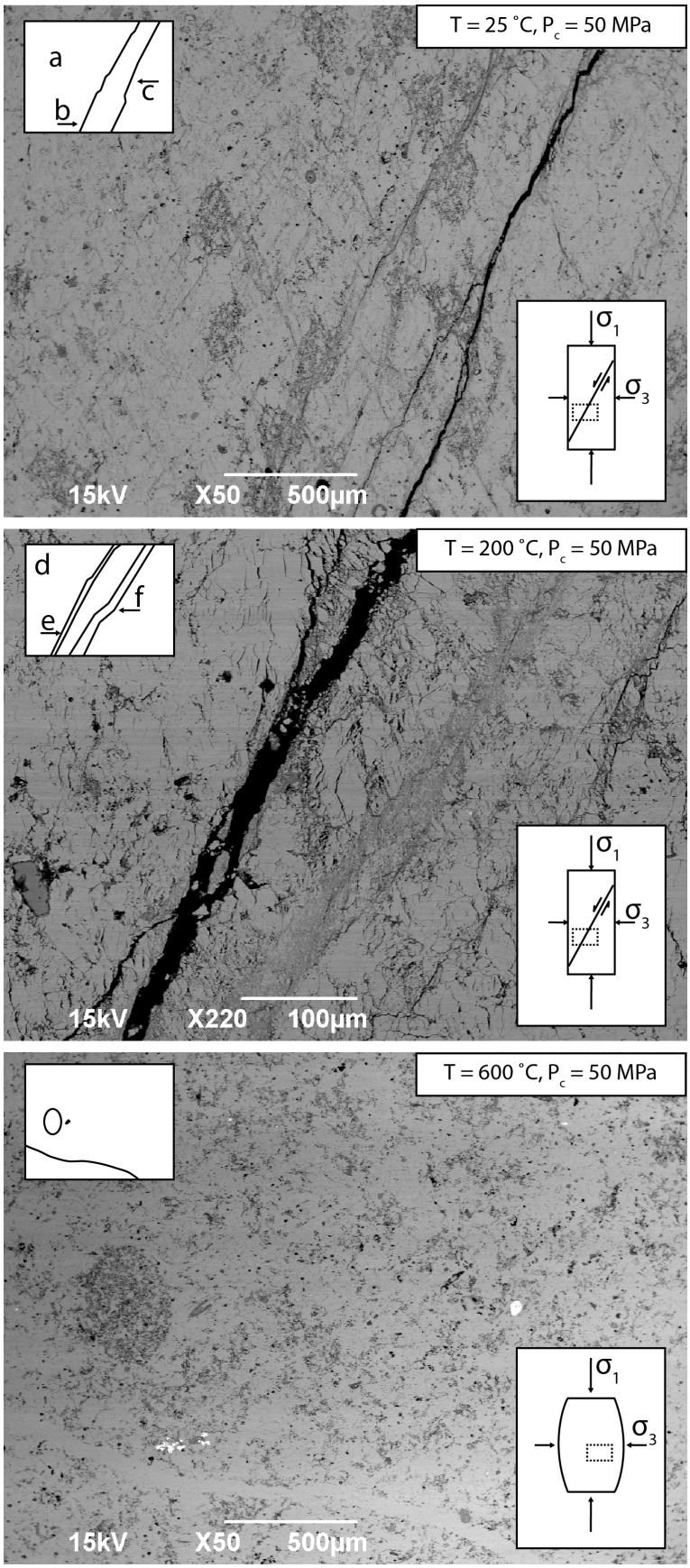

762

763 Figure 5 (color version, web usage)

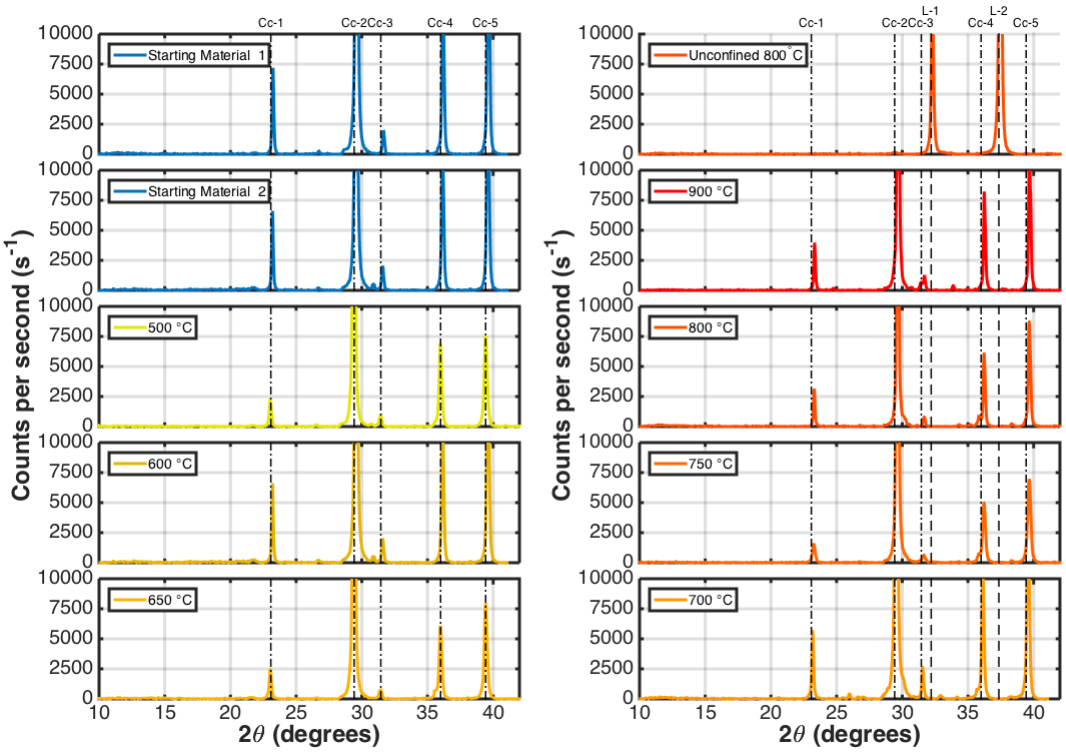

764

765 Figure 5 (grayscale, printed version)

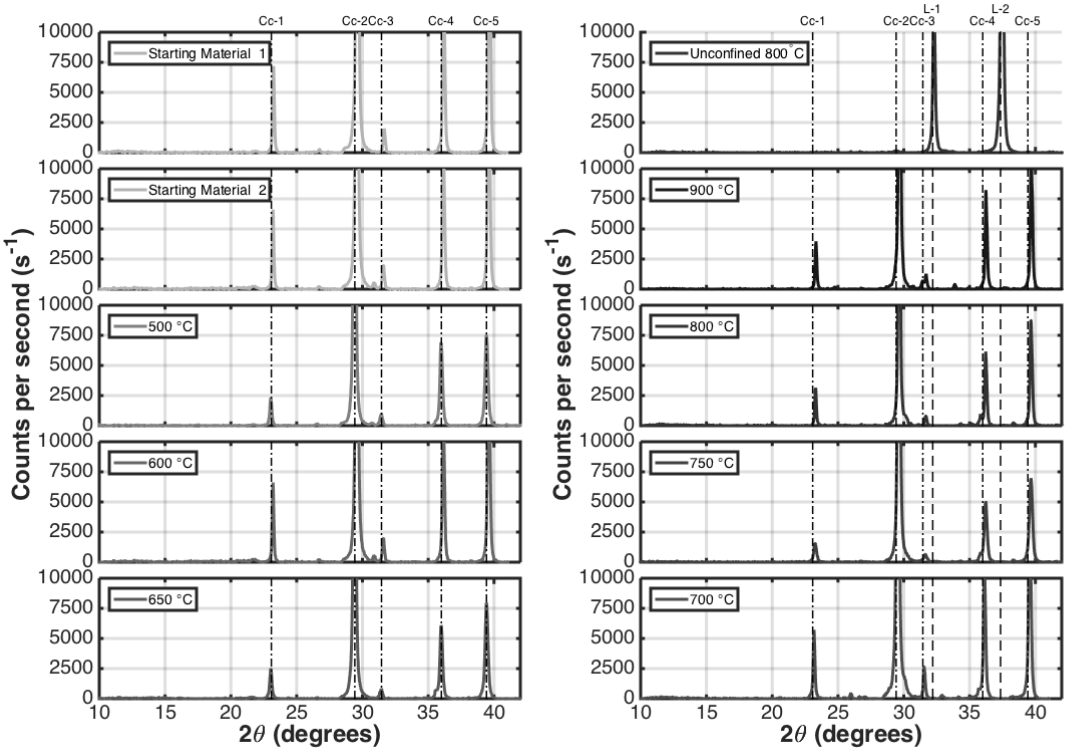

766

767

768 Figure 6 (color version, web usage)

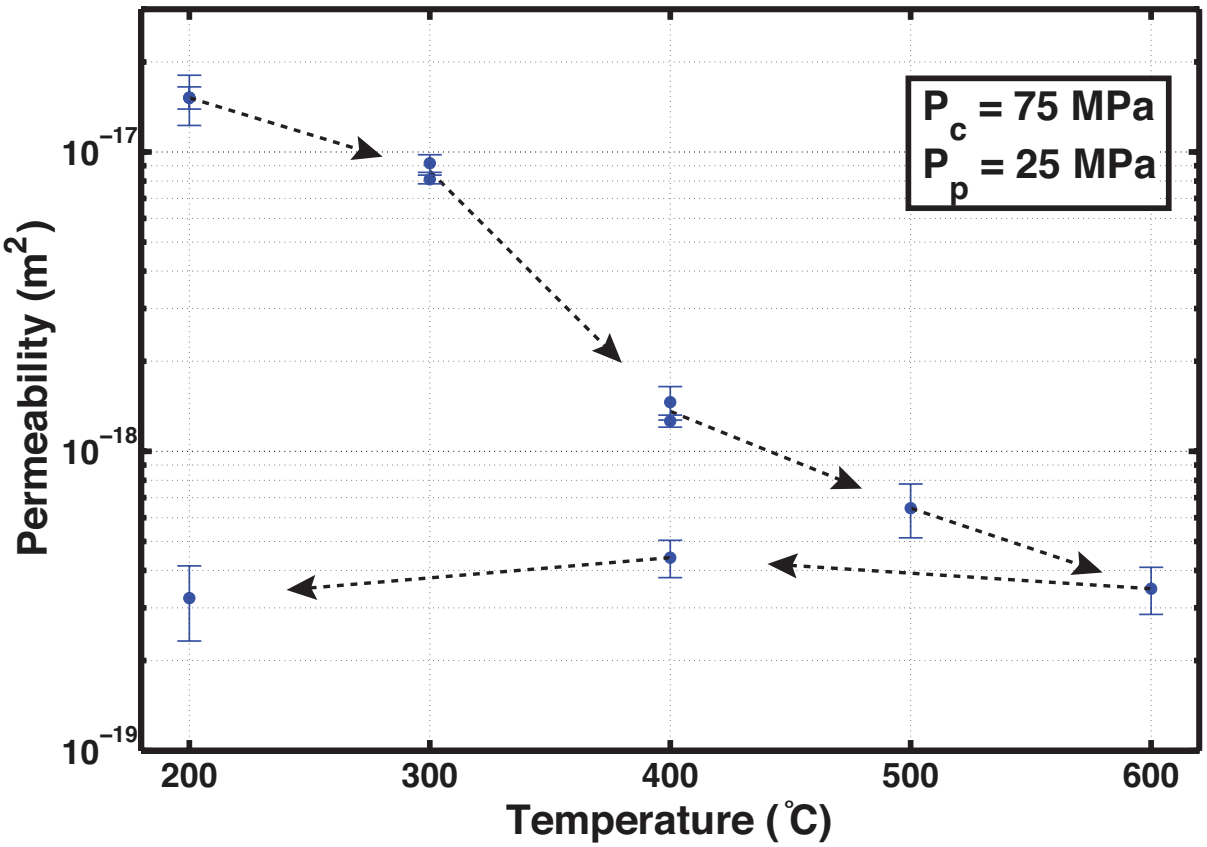

769

770 Figure 6 (grayscale, printed version)

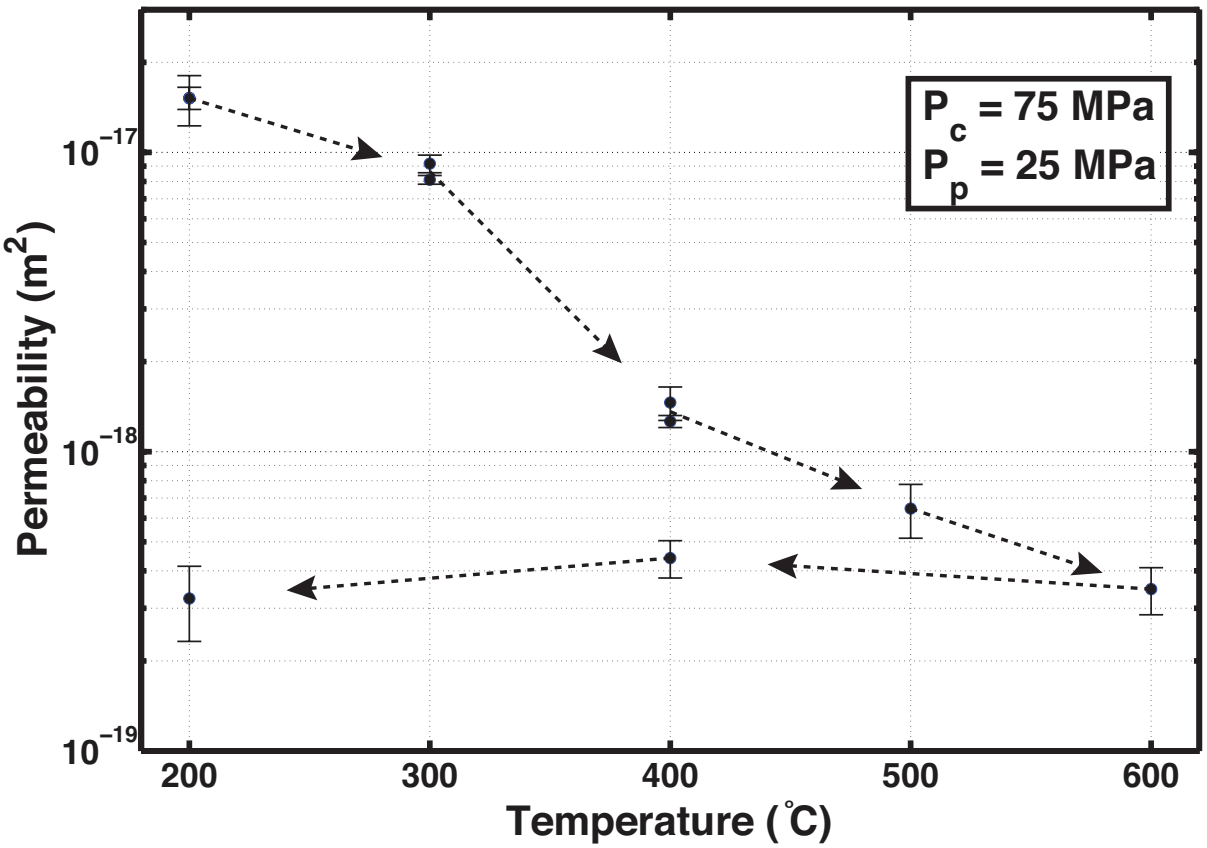
P_c = 75 MPa
P_p = 25 MPa
Permeability (m^2)
10^{-17}
10^{-18}
10^{-19}
200
300
400
500
600
Temperature (°C)

771

772

Supplementary material for:

Ductile flow in sub-volcanic carbonate basement as the main control for edifice stability new experimental insights

Richard R. Bakker*, Marie E.S. Violay, Philip M. Benson and Sergio C. Vinciguerra

* Corresponding author: R.R. Bakker, ETH Zürich, NO E 17, Sonneggstrasse 5, Zürich, CH-8092. (richard.bakker@erdw.ethz.ch)

This file includes the following:

1) List of preformed deformation experiments.
2) List of preformed other experiments (permeability and degassing)
3) Differential stress vs. strain curves comparing experiments at different confining pressure and temperature.

Supplementary item 1 - List of deformation experiments

In total 19 successful experiments were used in this study.

Table 1: Comprehensive list of experiments, listed here are: Experiment code, Temperature (˚C), Confining pressure (MPa), Jacket type (Shrink tube/Copper/Iron, ST/Cu/Fe), Yield point (% of strain where it occurred), Peak differential stress (if applicable), Differential stress at 5% total strain (MPa) (if applicable), note(s).

Exp. Code	Temp. (˚C)	Confining Pressure (MPa)	Jacket Mat.	Yield pt. (%)	Ultimate differential stress (MPa)	Differential stress at 5% strain	Open (O) / Closed (C)	Post Peak Behavior
P1596	25	50	ST	1.2	295	Not reached	C	Weakening (brittle failure)
P1600	25	100	ST	1.2	350	345	C	Weakening (brittle failure)
P1604	200	50	Cu	1.0	310	360	C	Weakening (brittle failure)
P1618	200	100	Cu	1.0	not reached	365	C	Weakening (brittle failure)
P1833	300	50	Cu	1.0	430	425	C	Weakening (brittle failure)
P1603	400	50	Cu	0.9	not reached	310	C	Hardening
P1715	400	100	Cu	0.9	not reached	350	C	Hardening
P1724	500	50	Cu	0.8	not reached	250	C	Hardening
P1606	600	50	Cu	0.6	not reached	180	C	Hardening
P1714	600	100	Cu	0.6	not reached	215	C	Hardening
P1710	600	50	Cu	0.6	not reached	210	O	Hardening
P1775	600	50	Cu	0.6	not reached	200	O	Hardening
P1774	600	50	Cu	0.6	not reached	195	C	Hardening
P1780	600	50	Cu	0.6	not reached	185	C	Hardening
P1831	800	50	Fe	<0.1	not reached	5	O	Hardening
P1832	800	50	Fe	<0.1	not reached	5	C	Hardening
P1830	900	50	Fe	<0.1	not reached	5	O	Hardening

Supplementary item 2 - List of permeability experiments

Table 2: overview of permeability and degassing experiments. Listed are: Experiment code, Temperature (˚C), Confining Pressure (MPa), Jacket material (Copper / Iron, Cu/Fe), Pore pressure and notes.

Exp. Code	Temperature (˚C)	Confining Pressure (MPa)	Jacket Mat.	Pore pressure (MPa)	Note(s)
P1769	200-600	75	Cu	25	Permeability test cycle
P1766	800	75	Fe	25	Impermeable, even with a 60 MPa Pressure difference

Supplementary item 3 – Differential stress vs. strain diagram

Differential stress (MPa) versus Strain (%) curves for Comiso Limestone for different temperatures at confining pressures of σ_3 = 50 MPa (dashed lines) and 100 MPa (solid lines). Comparative experiments were conducted at temperatures of 20 (blue), 200 (green), 400 (yellow) and 600 ˚C (red). All experiments were conducted using a constant strain rate of 10^{-5} s^{-1}.